Learning-based correction with Gaussian constraints for ghost imaging through dynamic scattering media

YANG PENG[1] AND WEN CHEN[1,2,*]

[1]*Department of Electrical and Electronic Engineering, The Hong Kong Polytechnic University, Hong Kong, China*
[2]*Photonics Research Institute, The Hong Kong Polytechnic University, Hong Kong, China*
*owen.chen@polyu.edu.hk

In this Letter, we propose a learning-based correction method to realize ghost imaging (GI) through dynamic scattering media using deep neural networks with Gaussian constraints. The proposed method learns the wave scattering mechanism in dynamic scattering environments, and rectifies physically-existing dynamic scaling factors in the optical channel. The corrected realizations obey Gaussian distributions, and can be used to recover high-quality ghost images. Experimental results demonstrate effectiveness and robustness of the proposed learning-based correction method, when imaging through dynamic scattering media is conducted. In addition, only the half number of realizations is needed in dynamic scattering environments, compared to that used in the temporally-corrected GI method. The proposed scheme provides a novel insight into GI, and could be a promising and powerful tool for optical imaging through dynamic scattering media.

The theory of ghost imaging (GI) was proposed in quantum domain [1]. It was further verified that GI can also be realized with classical light source [2]. In a typical GI setup, the illumination beam is split into two spatially correlated beams. One of the beams illuminates the object, and is detected by a single-pixel detector (SPD) without spatial resolution. The other beam does not interact with object, and impinges on a pixelated detector. The object information can be resolved by correlating the two sets of measurements. Later, spatial light modulator (SLM) is applied to modulate the light beam by controlling the pre-computed intensity pattern. Then, GI can be performed with only one beam [3]. Much effort has also been made to improve signal-to-noise ratio (SNR) of GI and shorten acquisition time, e.g., differential GI (DGI) [4], normalized GI [5], iterative GI [6], compressive sensing-based GI [7–9] and deep learning-based GI [10–14].

It has been demonstrated that GI with SPD has the capability against the destruction of light intensity distributions caused by scattering media. GI could achieve better performance than pixelated-sensor-based optical imaging techniques [15,16] in some environments, e.g., turbulence [17], underwater [18] and biological

tissues [19]. To date, most GI algorithms have been restricted to the experiments in static scattering media [10–14,17–19]. In a strongly dynamic scattering environment, dynamic scaling factors in the optical channel could induce remarkable correlation mismatches between illumination patterns and the realizations. Therefore, it is a great challenge to realize high-quality GI through dynamic scattering media. Recently, temporally corrected GI (TCGI) was studied [20], when the scattering medium is complex and dynamic. The number of realizations should be doubled in optical experiments, which dramatically increases acquisition time and prevents GI from developing into a more promising technique in dynamic and complex scenarios. It is desirable to develop novel strategies to correct dynamic scaling factors when taking the acquisition efficiency into consideration.

In this Letter, we propose a learning-based correction method to rectify dynamic scaling factors and recover high-fidelity ghost images in dynamic scattering media. Unlike current learning-based algorithms dedicated to mainly mitigating the impact of static scattering media, the proposed method learns dynamic scattering mechanism in turbid water via a digital way. A Gaussian constraint is also developed to correct the realizations to obey Gaussian distribution and effectively eliminate the influence of dynamic scaling factors. The simulated data generated for model training are based on the variation of dynamic scaling factors, and different turbidities of dynamic scattering environments are considered. When a series of realizations are recorded in dynamic scattering media to be tested, they can be corrected by using the trained model and then used to reconstruct high-quality object images. There is no limitation on the types of objects to be tested in optical experiments. The proposed learning-based correction method needs only the half number of realizations compared with the TCGI method, showing a great potential for the applications in various dynamic and complex scenarios.

In static environments, the physically-existing scaling factors in GI are usually assumed as a constant, and the realizations conform to Gaussian distribution when an object is sequentially illuminated by a series of illumination patterns [20]. The single-pixel detection process can be described by

$$B_{mn} = \int I_n(\mathbf{x}) G_m(\mathbf{x}) d\mathbf{x}, \tag{1}$$

where B_{mn} denotes a realization (i.e., one single-pixel light intensity) in GI, $m = 1, 2, ..., M$, M denotes the number of objects,

$n = 1, 2, ..., N$, N denotes the number of realizations, $I_n(\mathbf{x})$ denotes the series of illumination patterns with spatial coordinate $\mathbf{x}$, and $G_m(\mathbf{x})$ denotes the mth object transmission function. The scaling factor in Eq. (1) is usually assumed as a constant (e.g., 1) in static environments.

However, when imaging through dynamic scattering media is conducted, the dynamically-changed scaling factors could induce a significant fluctuation in the realizations. Gaussian distribution of the realizations is disrupted, and the object cannot be further recovered using GI methods. In the proposed learning-based correction method, the variation of dynamic scaling factors can be modeled. The variation of dynamic scaling factors at different turbidities of scattering environments can be represented by using different functions, e.g., exponential functions with different bases. Here, a neural network is designed to rectify dynamic scaling factors and obtain a series of corrected realizations. A Gaussian constraint is further incorporated into a loss function to optimize the neural network and facilitate the corrected realizations to obey Gaussian distributions.

The process of dataset generation in a digital way is shown in Fig. 1(a). For the training, 5000 objects $G \in \square^M$ with 128×128 pixels are selected from the Modified National Institute of Standards and Technology (MNIST) database to sequentially interact with a set of random patterns $I(\mathbf{x})$ in Eq. (1). A series of realizations $B \in \square^{M \times N}$ in static environments are obtained, which are normalized with $N = 16384$ for each object image. With an exponential transformation that emulates the variation of dynamic scaling factors $a \in \square^{M \times N}$ in this study, realizations $H \in \square^{M \times N}$ numerically generated in dynamic scattering environment, i.e., without the usage of labeled experimental data for the training, can be described by

$$H_{mn} = a_{mn} B_{mn} = k_m^t B_{mn}, \tag{2}$$

where $k \in \square^M$ denotes the base of exponential function, and t is the same as n. For each object, k is first selected randomly in a range (e.g., $[0.9995, 1]$) and then is fixed. The minimum value k is chosen based on the exponential curve of the realizations in practical, and k is not larger than 1 to ensure a downward trend of dynamic scaling factors. In various dynamic scattering media, parameters a_{mn} could be adjusted or designed to be adaptive.

The dataset for training is composed of the labeled pairs $S = (H; B, \sigma^2)$, where $\sigma^2 \in \square^M$ denotes the variance of realizations $B \in \square^{M \times N}$. It is worth noting that the series of realizations B and H for each object image is required to be reshaped to a $\sqrt{N} \times \sqrt{N}$ 2D image before being fed into the designed neural network. A framework of the proposed learning-based correction method is shown in Fig. 1(b). U-Net [21] is chosen as an architecture of the designed neural network. To estimate the corrected realizations Y, the designed neural network is optimized with the following loss functions.

$$Loss = L_{MSE} + L_G, \tag{3}$$

$$L_{MSE} = \frac{1}{MN} \sum_m \sum_n \left\| Y_{mn} - B_{mn} \right\|^2, \tag{4}$$

$$L_G = \frac{1}{MN} \sum_m \sum_n \left(\frac{1}{2} \left\{ \ln\left[\max\left(\sigma_m^2, eps\right) \right] + \frac{(Y_{mn} - B_{mn})^2}{\max(\sigma_m^2, eps)} \right\} \right), \tag{5}$$
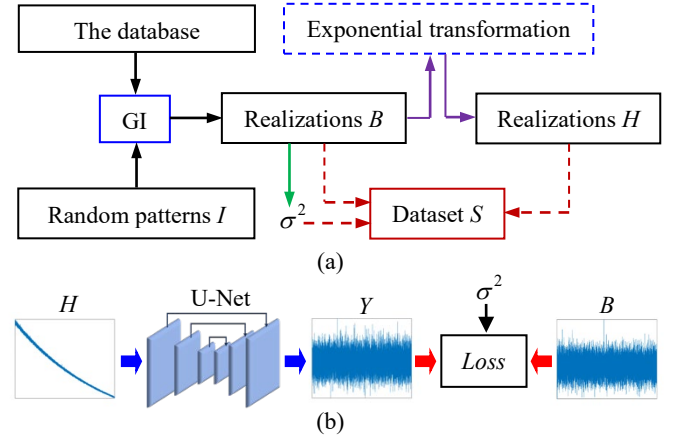

Fig. 1. (a) The process of dataset generation via a digital way in this study, σ^2: the variance of realizations B, and (b) schematic for a framework of the proposed learning-based correction method. B: the realizations to be numerically generated in static environments; H: the realizations emulated in dynamic scattering environments; Y: the corrected realizations.

where L_{MSE} denotes mean squared error (MSE), L_G denotes a Gaussian constraint function [22], ln denotes a natural logarithm, eps denotes a constant used for maintaining the training stability and its default is as 1.0×10^{-6}. It can be found that L_G can ensure the designed neural network to learn probability distribution of the realizations B. Therefore, the corrected realizations Y is constrained to be in accordance with a Gaussian distribution, and then can be further used to reconstruct a ghost image.

The training process is numerically implemented on a workstation with a NVIDIA GeForce RTX 1080 Ti GPU with codes in Pytorch. 100 epochs with a batch size of 16 are used. The learning rate is 0.0001, and Adam [23] is adopted as the optimizer. To reconstruct a ghost image with DGI, the corrected realizations Y generated by the trained neural network using the experimentally collected light intensities as inputs are reshaped to one row vector, and ghost reconstruction is further described by [4]

$$O(\mathbf{x}) = \left\langle \left(Y - \frac{\langle Y \rangle}{\langle Q \rangle} Q \right) \left(I(\mathbf{x}) - \langle I(\mathbf{x}) \rangle \right) \right\rangle, \tag{6}$$

where $O(\mathbf{x})$ denotes a recovered ghost image, $\langle . \rangle$ denotes an ensemble average, and $Q = \sum I(\mathbf{x})$.

A series of optical experiments are conducted through dynamic scattering media to verify the proposed learning-based correction method. In Fig. 2, a green laser beam with wavelength of 532.0 nm and maximum output power of 50.0 mW is expanded and collimated. 40000 random amplitude-only patterns with 128×128 pixels are sequentially embedded into an amplitude-only SLM (Holoeye, LC-R720) with a pixel size of 20.0 μm to be illuminated by the collimated beam. There is no requirement for random patterns. A 4f system with a focal length of 5.0 cm for L1 and a focal length of 10.0 cm for L2 is used to project random patterns onto the object. Diffraction limit in the optical setup is 40.0 μm, calculated by using pixel size of the SLM and the magnification factor of the 4f system. A transparent water tank (polymethyl
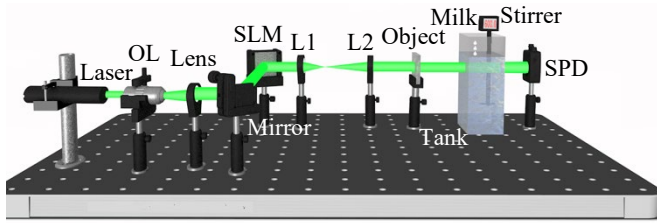
Fig. 2. A schematic experimental setup to verify the proposed method in dynamic scattering media. OL: objective lens; L1: a lens with a focal length of 5.0 cm; L2: a lens with a focal length of 10.0 cm.
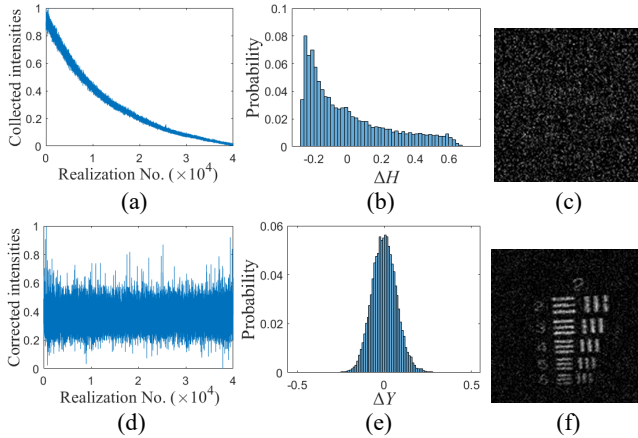

Fig. 3. (a) The experimentally-collected light intensities, (b) probability distribution corresponding to (a), (c) a reconstructed object using the realizations in (a), (d) the intensities corrected by using the proposed method, (e) probability distribution corresponding to (d), and (f) a reconstructed object using the realizations in (d).

methacrylate) with a dimension of 10.0 cm (Length) × 20.0 cm (Width) × 30.0 cm (Height) is placed in the optical path. 4000 ml clean water is placed in the water tank. Different volumes of skimmed milk diluted with 1000 ml clean water are kept dropping into water tank during optical experiments to create dynamic scattering environments with different turbidities. A stirrer rotates at 600 revolutions per minute (rpm). A single-pixel silicon photodiode (Thorlabs, PDA100A2) is used to record a range of light intensities. The axial distance between the object and SPD is 42.0 cm, and the axial distance between the front face of water tank and SPD is 36.0 cm.

A USAF 1951 resolution test chart is used as the object in Fig. 2 to test spatial resolution achieved by the proposed learning-based correction method in dynamic scattering media. 10 ml skimmed milk diluted with 1000 ml clean water is kept dropping into water tank over 66.7 minutes. The curve of collected single-pixel light intensities after normalization is shown in Fig. 3(a) which shows an exponential-like downward trend. The significant variance of collected intensities indicates the influence of dynamic scaling factors, which matches the model designed in the digital dataset generation. The collected intensities do not obey Gaussian distribution, as shown in Fig. 3(b). Here, ΔH is denoted by the experimentally-collected light intensities minus mean value of the experimentally-collected light intensities. The recovery result
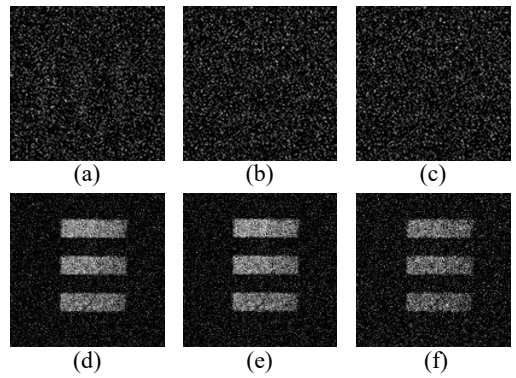

Fig. 4. The experimentally recovered ghost images obtained when 10 ml, 20 ml, and 30 ml skimmed milk is respectively used: (a)-(c) DGI, and (d)-(f) the proposed learning-based correction method.

using the realizations in Fig. 3(a) with DGI is shown in Fig. 3(c). No information about the object can be observed, showing that conventional method fails to work in dynamic scattering environments. When the proposed learning-based correction method is applied, the corrected light intensities in Fig. 3(d) fluctuate in a certain range. It is demonstrated that effect of dynamic scaling factors is eliminated with the proposed method. The corrected intensities obey the property of Gaussian distribution with Gaussian constraints designed in the proposed method, as shown in Fig. 3(e). Here, ΔY is denoted by the corrected intensities minus mean value of the corrected intensities. When the corrected intensities in Fig. 3(d) are used to reconstruct a ghost image with DGI, experimental result is shown in Fig. 3(f). It can be found that the object information of Group 2 in the USAF 1951 resolution test chart can be recovered with high quality. The element 6 in Group 2 can be clearly identified and resolved. Therefore, spatial resolution achieved is 70.15 μm in the proposed method, when imaging in the dynamic and complex environment is conducted.

To demonstrate robustness of the proposed method in dynamic scattering environments, the influence of different volumes of skimmed milk is further tested based on the experimental setup in Fig. 2. Triple-bar in USAF 1951 element 2 of Group 0 is used as an object. The experimentally-collected single-pixel intensities and single-pixel intensities corrected by the proposed method are shown in Fig. S1 in Supplement 1. The corresponding probability distributions are shown in Fig. S2 in Supplement 1. It can be found that the impact of dynamic scattering media is more obvious with an increase of the volume of skimmed milk. The collected intensities fail to conform to Gaussian distribution regardless of the volumes of milk. When the proposed learning-based correction method is used, the influence of different turbidities of dynamic scattering environments can be fully suppressed and probability distributions of the corrected intensities are in accordance with Gaussian.

Typically recovered experimental results are shown in Fig. 4 when 10 ml, 20 ml and 30 ml skimmed milk is used, respectively. The reconstructed ghost images with DGI have no any effective information, as shown in Figs. 4(a)–4(c). When the proposed learning-based method is applied to rectify dynamic scaling factors, the recovered ghost images are of high fidelity, as shown in Figs. 4(d)–4(f). Quality of the recovered ghost images is quantitatively

evaluated by using SNR [24] [see Eq. (S1) in Supplement 1]. Figure 5 shows SNR values of the recovered ghost images, when different volumes of skimmed milk are used in DGI method and the proposed method. When no milk (i.e., 0 ml) is dropped into water tank during optical experiments, it is feasible for DGI and the proposed learning-based correction method to recover high-quality ghost images. SNR values are 2.87 and 3.57, respectively. When milk is dropped into water tank, SNR values of the recovered ghost images using conventional DGI are nearly 0. With the proposed learning-based correction method, the SNR value can stabilize at a high level, when the volume of milk ranges from 0 ml to 20.0 ml. Although quality of the recovered ghost image decreases as the volume of milk increases to 30.0 ml, effective object information can still be obtained, as shown in Fig. 4(f). Experimental results in Fig. 5 show high robustness of the proposed learning-based correction method against different degrees of dynamic scattering. Other different objects have been tested in this study, and similar SNR trends are obtained.
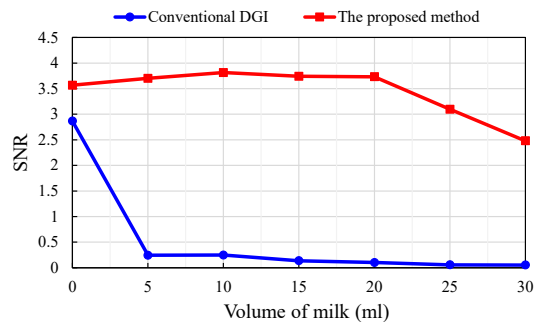

Fig. 5. A variation of SNR values of the experimentally recovered ghost images using DGI method and the proposed learning-based correction method, when different volumes of skimmed milk are individually used in Fig. 2.

Conventional learning-based algorithms usually have a limited generalization, since the performance is satisfactory only when the object to be experimentally tested is close to those in the training dataset. The proposed learning-based correction method can overcome this drawback by learning the dynamic scattering mechanism in the realizations via a digital way, rather than just mapping the degraded images to clean images. High-fidelity experimental results can still be obtained, when the objects to be tested (e.g., USAF 1951 resolution test chart) are different from those in the database. In various dynamic scattering media, the fitting or parameters in Eq. (2) can also be adjusted or designed to be adaptive. The proposed method has a high generalization for different objects (e.g., binary and grayscale) placed in the optical path, when there is a dynamic scattering environment. Furthermore, the proposed method has an advantage of removing the usage of temporal carriers in TCGI [20] in dynamic scattering media. Only the half number of realizations is required compared with TCGI, which can improve efficiency of data acquisition. Different volumes of milk have been studied, and the high-fidelity recovered ghost images illustrate high robustness of the proposed method. Since the influence of light wavelength (e.g., red laser) and the stirrer speed (e.g., 200.0 rpm to 1500.0 rpm) are trivial, the analysis is omitted here.

In conclusion, we have proposed a learning-based correction method to realize high-fidelity GI through dynamic scattering media by correcting the physically-existing dynamic scaling factors in the optical channel. A Gaussian constraint is also taken into consideration in the loss function of the designed neural network, and corrected intensities are in accordance with Gaussian distributions. Experimental results demonstrate that the proposed learning-based correction method is effective and robust without extra temporal carriers to be used in the optical setup. It can be expected that this work could have a great application prospect for GI in a wide range of free-space wave propagation environments, and a foundation has been laid for a further reduction of the number of realizations.

REFERENCES

1. T. B. Pittman, Y. H. Shih, D. V. Strekalov, and A. V. Sergienko, Phys. Rev. A **52**, 3429 (1995).
2. A. Gatti, E. Brambilla, M. Bache, and L. A. Lugiato, Phys. Rev. Lett. **93**, 093602 (2004).
3. J. H. Shapiro, Phys. Rev. A **78**, 061802 (2008).
4. F. Ferri, D. Magatti, L. A. Lugiato, and A. Gatti, Phys. Rev. Lett. **104**, 253603 (2010).
5. B. Sun, S. S. Welsh, M. P. Edgar, J. H. Shapiro, and M. J. Padgett, Opt. Express **20**, 16892 (2012).
6. W. Wang, Y. P. Wang, J. Li, X. Yang, and Y. Wu, Opt. Lett. **39**, 5150 (2014).
7. O. Katz, Y. Bromberg, and Y. Silberberg, Appl. Phys. Lett. **95**, 131110 (2009).
8. W. Yu, M. Li, X. Yao, X. Liu, L. Wu, and G. Zhai, Opt. Express **22**, 7133 (2014).
9. P. Zerom, K. W. C. Chan, J. C. Howell, and R. W. Boyd, Phys. Rev. A. **84**, 061804 (2011).
10. F. Wang, H. Wang, H. Wang, G. Li, and G. Situ, Opt. Express **27**, 25560 (2019).
11. F. Li, M. Zhao, Z. Tian, F. Willomitzer, and O. Cossairt, Opt. Express **28**, 17395 (2020).
12. Z. Gao, X. Cheng, J. Yue, and Q. Hao, Opt. Express **30**, 45759 (2022).
13. H. Liu, Y. Chen, L. Zhang, D. Li, and X. Li, Opt. Lett. **47**, 569 (2022).
14. M. Lyu, W. Wang, H. Wang, H. Wang, G. Li, N. Chen, and G. Situ, Sci. Rep. **7**, 17865 (2017).
15. I. M. Vellekoop and A. P. Mosk, Opt. Lett. **32**, 2309 (2007).
16. S. M. Popoff, G. Lerosey, R. Carminati, M. Fink, A. C. Boccara, and S. Gigan, Phys. Rev. Lett. **104**, 100601 (2010).
17. R. E. Meyers, K. S. Deacon, and Y. Shih, Appl. Phys. Lett. **98**, 111115 (2011).
18. M. Le, G. Wang, H. Zheng, J. Liu, Y. Zhou, and Z. Xu, Opt. Express **25**, 22859 (2017).
19. W. Huang, W. Tan, H. Qin, J. Wang, Z. Huang, X. Huang, X. Fu, and Y. Bai, J. Opt. Soc. Am. B **40**, 1696 (2023).
20. Y. Xiao, L. Zhou, and W. Chen, Opt. Lett. **47**, 3692 (2022).
21. O. Ronneberger, P. Fischer, and T. Brox, in *Proceedings of the 18th International Conference on Medical Image Computing and Computer-Assisted Intervention – MICCAI 2015*, 234 (2015).
22. D. A. Nix and A. S. Weigend, in *Proceedings of 1994 IEEE International Conference on Neural Network (ICNN'94)*, 55 (1994).
23. D. P. Kingma and J. Ba, in *Proceedings of the 3rd International Conference on Learning Representations* (2015).
24. B. Redding, M. A. Choma, and H. Cao, Nat. Photonics **6**, 355 (2012).

References with full titles

1. T. B. Pittman, Y. H. Shih, D. V. Strekalov, and A. V. Sergienko, "Optical imaging by means of two-photon quantum entanglement," Phys. Rev. A **52**, 3429–3432 (1995).

2. A. Gatti, E. Brambilla, M. Bache, and L. A. Lugiato, "Ghost imaging with thermal light: comparing entanglement and classical correlation," Phys. Rev. Lett. **93**, 093602 (2004).

3. J. H. Shapiro, "Computational ghost imaging," Phys. Rev. A **78**, 061802 (2008).

4. F. Ferri, D. Magatti, L. A. Lugiato, and A. Gatti, "Differential ghost imaging," Phys. Rev. Lett. **104**, 253603 (2010).

5. B. Sun, S. S. Welsh, M. P. Edgar, J. H. Shapiro, and M. J. Padgett, "Normalized ghost imaging," Opt. Express **20**, 16892–16901 (2012).

6. W. Wang, Y. P. Wang, J. Li, X. Yang, and Y. Wu, "Iterative ghost imaging," Opt. Lett. **39**, 5150–5153 (2014).

7. O. Katz, Y. Bromberg, and Y. Silberberg, "Compressive ghost imaging," Appl. Phys. Lett. **95**, 131110 (2009).

8. W. Yu, M. Li, X. Yao, X. Liu, L. Wu, and G. Zhai, "Adaptive compressive ghost imaging based on wavelet trees and sparse representation," Opt. Express **22**, 7133–7144 (2014).

9. P. Zerom, K. W. C. Chan, J. C. Howell, and R. W. Boyd, "Entangled-photon compressive ghost imaging," Phys. Rev. A. **84**, 061804 (2011).

10. F. Wang, H. Wang, H. Wang, G. Li, and G. Situ, "Learning from simulation: an end-to-end deep-learning approach for computational ghost imaging," Opt. Express **27**, 25560–25572 (2019).

11. F. Li, M. Zhao, Z. Tian, F. Willomitzer, and O. Cossairt, "Compressive ghost imaging through scattering media with deep learning," Opt. Express **28**, 17395–17408 (2020).

12. Z. Gao, X. Cheng, J. Yue, and Q. Hao, "Extendible ghost imaging with high reconstruction quality in strong scattering medium," Opt. Express **30**, 45759–45775 (2022).

13. H. Liu, Y. Chen, L. Zhang, D. Li, and X. Li, "Color ghost imaging through the scattering media based on A-cGAN," Opt. Lett. **47**, 569–572 (2022).

14. M. Lyu, W. Wang, H. Wang, H. Wang, G. Li, N. Chen, and G. Situ, "Deep-learning-based ghost imaging," Sci. Rep. **7**, 17865 (2017).

15. I. M. Vellekoop and A. P. Mosk, "Focusing coherent light through opaque strongly scattering media," Opt. Lett. **32**, 2309–2311 (2007).

16. S. M. Popoff, G. Lerosey, R. Carminati, M. Fink, A. C. Boccara, and S. Gigan, "Measuring the transmission matrix in optics: an approach to the study and control of light propagation in disordered media," Phys. Rev. Lett. **104**, 100601 (2010).

17. R. E. Meyers, K. S. Deacon, and Y. Shih, "Turbulence-free ghost imaging," Appl. Phys. Lett. **98**, 111115 (2011).

18. M. Le, G. Wang, H. Zheng, J. Liu, Y. Zhou, and Z. Xu, "Underwater computational ghost imaging," Opt. Express **25**, 22859–22868 (2017).

19. W. Huang, W. Tan, H. Qin, J. Wang, Z. Huang, X. Huang, X. Fu, and Y. Bai, "Edge detection based on ghost imaging through biological tissue," J. Opt. Soc. Am. B **40**, 1696–1702 (2023).

20. Y. Xiao, L. Zhou, and W. Chen, "High-resolution ghost imaging through complex scattering media via a temporal correction," Opt. Lett. **47**, 3692–3695 (2022).

21. O. Ronneberger, P. Fischer, and T. Brox, "U-Net: convolutional networks for biomedical image segmentation," in *Proceedings of the 18th International Conference on Medical Image Computing and Computer-Assisted Intervention – MICCAI 2015*, 234–241 (2015).

22. D. A. Nix and A. S. Weigend, "Estimating the mean and variance of the target probability distribution," in *Proceedings of 1994 IEEE International Conference on Neural Network (ICNN'94)*, 55–60 (1994).

23. D. P. Kingma and J. Ba, "Adam: A method for stochastic optimization," in *Proceedings of the 3rd International Conference on Learning Representations* (2015).

24. B. Redding, M. A. Choma, and H. Cao, "Speckle-free laser imaging using random laser illumination," Nat. Photonics **6**, 355–359 (2012).